CANCER BIOLOGY

# Schedule-dependent interaction between anticancer treatments

Sheng-hong Chen,[1] William Forrester,[2] Galit Lahav[1]

**The oncogene *MDMX* is overexpressed in many cancers, leading to suppression of the tumor suppressor p53. Inhibitors of the oncogene product MDMX therefore might help reactivate p53 and enhance the efficacy of DNA-damaging drugs. However, we currently lack a quantitative understanding of how MDMX inhibition affects the p53 signaling pathway and cell sensitivity to DNA damage. Live cell imaging showed that MDMX depletion triggered two distinct phases of p53 accumulation in single cells: an initial postmitotic pulse, followed by low-amplitude oscillations. The response to DNA damage was sharply different in these two phases; in the first phase, MDMX depletion was synergistic with DNA damage in causing cell death, whereas in the second phase, depletion of MDMX inhibited cell death. Thus a quantitative understanding of signal dynamics and cellular states is important for designing an optimal schedule of dual-drug administration.**

Efficient killing of cancer cells often requires combinations of drugs. A major rationale underlying such approaches is that the administration of two drugs that work through different mechanisms should reduce overall drug resistance and increase tumor eradication. A related combinatorial therapy approach is to apply anticancer drugs sequentially (*1*, *2*). In this case, treatment with the first drug may modify ("rewire") the behavior of specific signaling pathways, resulting in a population of cancer cells that is more sensitive to the second treatment (*1*). Improving the efficacy of time-staggered combinatorial treatments and designing optimal schedules require a detailed quantitative understanding of how each treatment dynamically alters cellular states in individual cells.

We investigated how weakening the effects of the oncogene product MDMX (also known as MDM4 and HDMX) alters the state of individual cancer cells and how these changes affect their sensitivity to DNA damage over time. *MDMX* is amplified in many tumors, including melanoma, osteosarcoma, and breast and colorectal cancers. Overexpression of MDMX inhibits the tumor-suppressive effects of the protein p53 and leads to resistance to anticancer drugs (*3*, *4*). Antagonization of MDMX may therefore enhance the efficacy of DNA-damaging drugs (*3*, *5*). Effects of MDMX on the abundance of p53 have been measured at one or a few time points in populations of cells (*6*–*8*). However, it remains unclear how MDMX regulates the dynamics of p53, which is important in determining a cell's response to DNA damage (*9*). We examined the effects of MDMX inhibition on p53 dynamics and the susceptibility to DNA damage in individual cells.

Multiple MDMX inhibitors are under development (*10*, *11*), but the specificity and efficacy of candidate inhibitors are still under study. We therefore used small interfering RNA (siRNA) to inhibit MDMX. Immunoblots showed that amounts of MDMX were effectively reduced in cells treated with siRNA (Fig. 1, A and B), leading to a transient increase in the amount of p53, followed by a decrease below its initial basal levels (Fig. 1, A and B). Population averages were previously shown to mask p53 dynamics in single cells (*12*, *13*). We therefore quantified p53 dynamics in individual cells after MDMX depletion in a p53 reporter cell line (Fig. 1, C and D, and experimental procedures). Cells transfected with scrambled siRNA showed a pulse of p53 accumulation after mitosis, as previously reported for actively dividing cells [Fig. 1E and (*13*)]. Cells transfected with MDMX siRNA also showed this postmitotic pulse (Fig. 1F) with a similar length but larger amplitude (Fig. 1, I and J). Most cells showed the p53 postmitotic pulse within the first 25 hours, which is consistent with their cell cycle length (fig. S1A). In our experimental conditions, division time was not synchronized between individual cells (Fig. 1H); therefore, each cell showed the postmitotic pulse at a different time, giving the appearance of a prolonged increase in p53 immunoblots representing the population average (Fig. 1B). After the initial postmitotic p53 pulses, cells depleted of MDMX showed oscillations in p53 abundance that persisted during the course of the experiment (60 hours; Fig. 1, F and H). The amplitude of these oscillations was lower than that of the spontaneous p53 pulses in dividing cells expressing MDMX (Fig. 1J), leading to lower overall amounts of p53 in the cell population (Fig. 1, A and B). The response to MDMX depletion therefore has two phases in individual cells: During the first phase, cells show a high-amplitude p53 pulse, and during the second phase, cells experience low-amplitude p53 oscillations. Because these dynamics are triggered after division, each cell enters the first and second phase of the response at a different time (Fig. 1H). Similar biphasic p53 dynamics were also found in the noncancerous primary line RPE1 (fig. S2), suggesting that these MDMX-mediated dynamics are not limited to cancer cells. The p53 postmitotic pulse appeared in RPE1 within 20 hours, which is consistent with their shorter cell cycle length (fig. S1B).

The p53 oscillations during the second phase of the response resemble the p53 oscillations that occur in response to DNA double-strand breaks (DSBs) (*14*). Although the p53 oscillations resulting from MDMX depletion had lower amplitude than those induced by DSBs (MCF7: Fig. 1, G and L; RPE1: fig. S2, C and H), both shared a remarkably similar period (Fig. 1K and fig. S2G). We therefore suggest that MDMX-mediated p53 oscillations result from the core negative feedback loop between p53 and Mdm2, as was previously suggested after DNA damage [Fig. 1M and (*14*)]. Mdm2 suppression led to completely different non-oscillatory p53 dynamics (fig. S3), strengthening the model that Mdm2 is required for p53 oscillations after DNA damage and MDMX suppression. The similarity in oscillation period led us to ask whether the p53 oscillations after MDMX knockdown result from activation of the DNA-damage signaling pathway. We measured the abundance of gamma-H2AX, an indicator of DSBs, in cells transfected with scrambled or MDMX siRNA and found that MDMX depletion did not increase the gamma-H2AX signal (Fig. 1, N and O). There was also no change in the phosphorylation states of the two major DNA-damage effector kinases, Chk1 and Chk2, after MDMX knockdown (Fig. 1P), suggesting that p53 oscillations after MDMX depletion do not result from DNA-damage signaling.

We used a cell line expressing a fluorescently tagged p53 and an inducible *MDMX* fused to mKate2 (a far-red fluorescent protein) to quantify p53 dynamics after reintroducing MDMX during the oscillatory phase (Fig. 2, A to D). The addition of doxycycline led to increased amounts of mKate2-MDMX (Fig. 2, B and D), which suppressed p53 oscillations (Fig. 2E), suggesting that MDMX prevents p53 oscillations in nonstressed conditions. Amounts of MDMX decreased in response to DSBs [fig. S4A and (*15*)], raising the possibility that a decreased abundance of MDMX is required for p53 oscillations. To examine the effect of MDMX on p53 oscillations that result from DSBs, we triggered DSBs with the radiomimetic drug neocarzinostatin (NCS) and measured p53 dynamics before and after expression of mKate2-MDMX. NCS led to p53 oscillations (*16*), and accumulation of mKate2-MDMX again diminished p53 oscillations (Fig. 2F). Incubation of cells with doxycycline before treatment with NCS dampened the NCS-induced p53 oscillations (Fig. 2, G and H, and fig. S4B). Thus, MDMX suppresses p53 oscillations both in basal conditions and in cells with DSBs. MDMX degradation after DSBs is required to allow p53 oscillations.

To determine the effects of the two-phase p53 response after MDMX depletion on the transcription of p53 target genes, we quantified the amounts of transcripts of well-characterized p53 target genes in different cellular programs.

[1]Department of Systems Biology, Harvard Medical School, Boston, MA, USA. [2]Developmental and Molecular Pathways, Novartis Institutes for Biomedical Research, Cambridge, MA, USA.

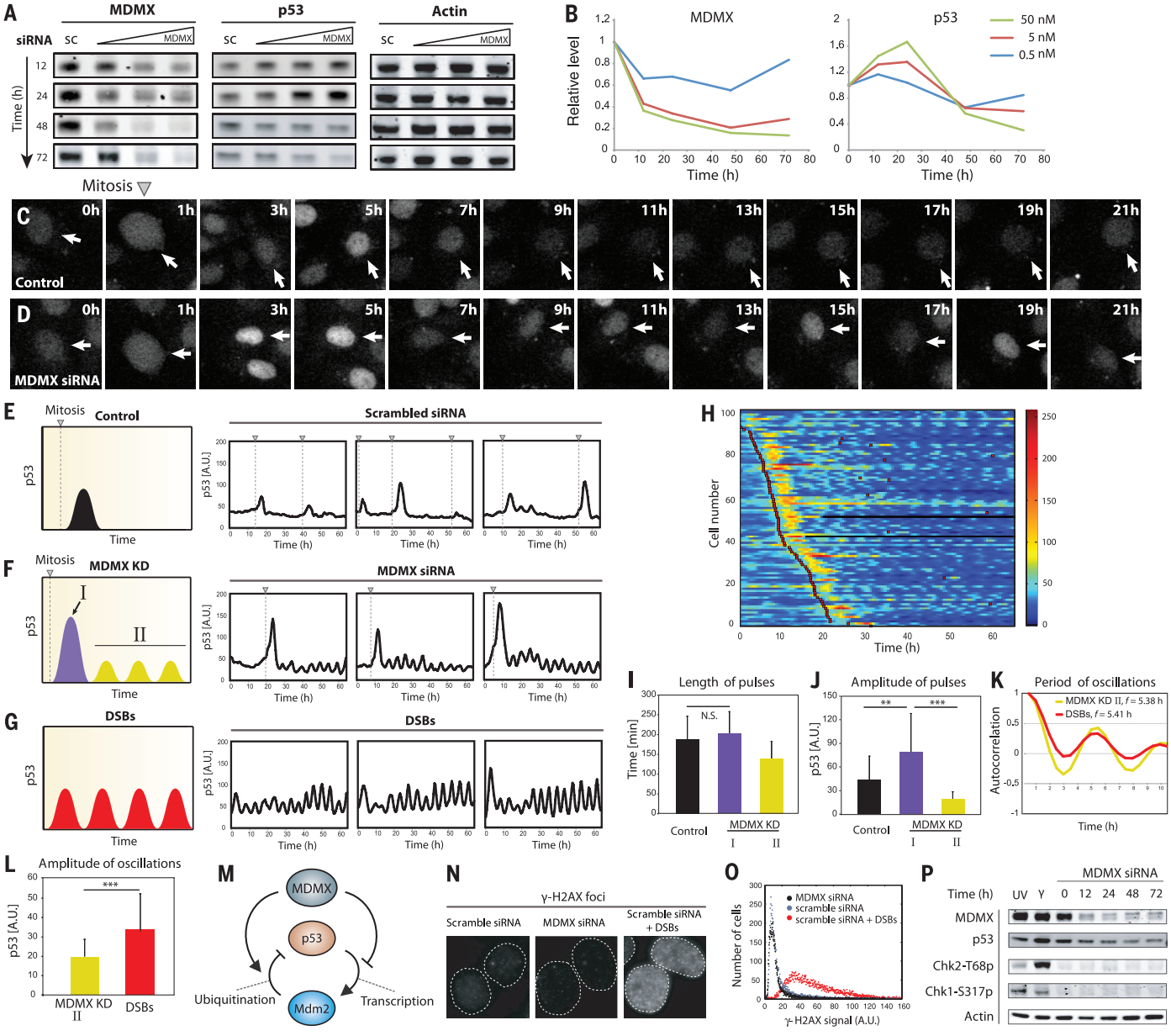


**Fig. 1. Single cells show two phases of p53 dynamics after MDMX depletion.** (**A**) Abundance of MDMX, p53, and actin in Western blots of extracts from MCF7 cells transfected with either scrambled siRNA (sc, 5 nM) or siRNA targeting MDMX's mRNA (0.5, 5, and 50 nM) for the indicated times. (**B**) Quantification of MDMX and p53 abundance from (A). The amount of siRNA used is shown in the upper right corner. (**C** and **D**) Time-lapse microscopy images of cells expressing p53-mCerulean after transfection with scrambled (C) or MDMX (D) siRNAs. (**E**, **F**, and **G**) Abundance of p53 in individual cells tracked as fluorescence of p53-mCerulean. Triangles with dashed lines indicate cell division. and p53-mCerulean dynamics in MDMX knockdown cells are classified into phase I (first postmitotic pulse) and phase II (low-amplitude oscillations). DSBs were introduced by NCS. Illustrations on the left summarize p53 dynamics. (**H**) Heat map of p53-mCerulean abundance in cells treated with MDMX siRNA. p53 traces of individual cells are arranged from top to bottom by the occurrence of first mitosis. Red squares indicate the time of cell division. (**I**) The mean relative widths measured by full width at half maximum [$n > 90$ p53 pulses; error bars indicate SD; the two p53 postmitotic pulses are not statistically significantly different ($P = 0.14$; $P$ values obtained by Student's two-sample unequal variance $t$ test, with a two-tailed distribution)]. (**J**) Amplitude of p53 pulses in control cells and MDMX KD cells [$n > 90$ p53 pulses; error bars indicate SD; $^{**}P < 10^{-8}$, $^{***}P < 10^{-19}$ ($P$ values obtained by Student's two-sample unequal variance t test, with a two-tailed distribution)]. (**K**) Periods of p53 oscillations in MDMX knockdown (phase II) and NCS-treated cells measured by autocorrelation. (**L**) The mean relative amplitudes of p53 oscillations in MDMX knockdown (phase II) and NCS-treated cells are shown ($n > 90$ p53 pulses; error bars indicate SD, $^{***}P < 10^{-19}$ ($P$ values obtained by Student's two-sample unequal variance $t$ test, with a two-tailed distribution)]. A.U., arbitrary units. (**M**) A schematic diagram of MDMX regulating p53. p53 oscillations were previously shown to result from the p53-Mdm2 negative feedback loop. MDMX acts to inhibit the p53-Mdm2 oscillator through two arms: One arm inhibits p53 transcriptional activity (right arm) and the second arm degrades p53 through catalyzing Mdm2-mediated p53 ubiquitination (left arm). (**N** and **O**) The γ-H2AX signal is shown (N) and quantified (O) in MCF7 cells transfected with either scrambled or MDMX siRNAs, followed by NCS treatment. (**P**) The abundance of indicated proteins in MCF7 cells either ultraviolet- or γ-irradiated or transfected with MDMX siRNA for the indicated times, analyzed by Western blot.

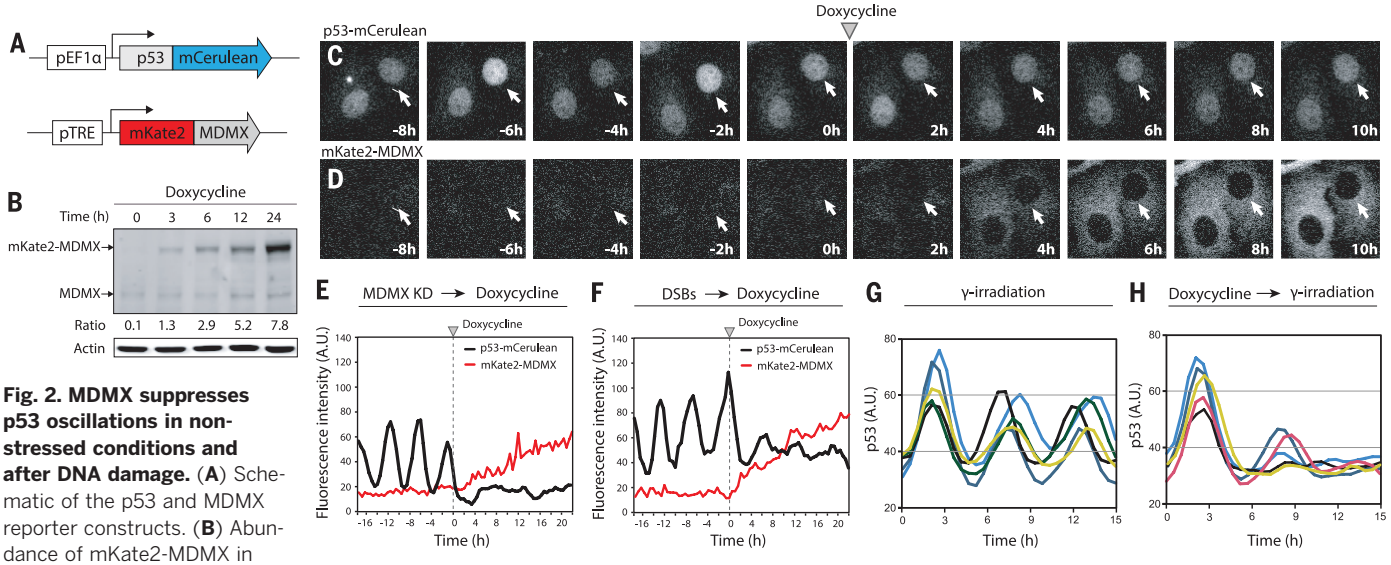


**Fig. 2. MDMX suppresses p53 oscillations in non-stressed conditions and after DNA damage.** (**A**) Schematic of the p53 and MDMX reporter constructs. (**B**) Abundance of mKate2-MDMX in p53-MDMX reporter cells treated with doxycycline, analyzed by Western blot. pEF1α, EF1 alpha promoter; pTRE, Tet response element promoter. (**C** and **D**) Time-lapse microscopy images of p53-mCerulean (C) and mKate2-MDMX (D) after MDMX siRNAs (30 hours), followed by doxycycline. (**E** and **F**) Trajectories of p53-mCerulean and mKate2-MDMX levels are shown for cells with either MDMX knockdown (E) or NCS (F) treatment 30 hours before doxycycline addition. (**G** and **H**) Trajectories of p53-mCerulean levels are shown for cells treated with NCS alone (G) or with prior treatment of doxycycline (H).

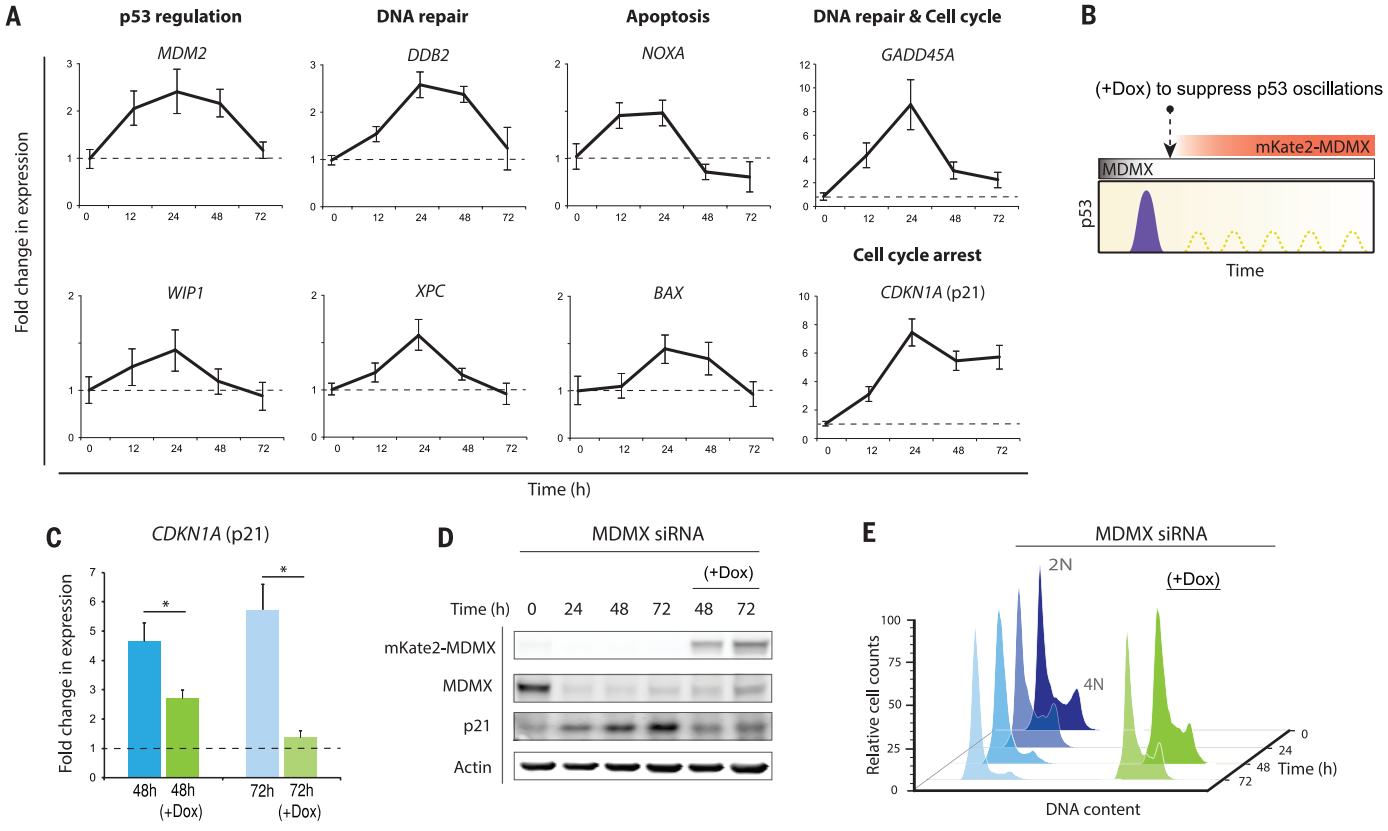


**Fig. 3. p53 oscillations during phase II are required to maintain p21 accumulation and cell cycle arrest.** (**A**) Expression of p53 target genes measured by quantitative polymerase chain reaction after MDMX knockdown. Genes are grouped according to their function ($n = 3$ biological repeats; error bars represent SD). (**B**) Schematic of suppressing p53 oscillations by inducing mKate2-MDMX using doxycycline. Doxycycline was added 24 hours after MDMX siRNA transfection. (C) Abundance of transcripts of *CDKN1A* (p21) 2 and 3 days after MDMX siRNA transfection alone or followed by doxycycline addition [$n = 3$ biological repeats; error bars indicate SD, $^{*}P < 10^{-2}$ ($P$ values obtained by Student's two-sample unequal variance $t$ test, with a two-tailed distribution)]. (**D**) Abundance of p21 protein in cells depleted of MDMX alone or with doxycycline addition. (**E**) Cell cycle profile after MDMX depletion alone or with doxycycline addition.

Most p53 targets showed a mild transient increase in transcription after MDMX depletion in the first 24 to 48 hours, and returned to their basal levels by 72 hours (Fig. 3A). These genes may be sensitive to the first-phase postmitotic pulse of p53 after MDMX depletion, but less sensitive to the second oscillatory phase of p53. The behavior of *CDKN1A*, a gene encoding p21 (cyclin-dependent kinase inhibitor 1), was distinct. Amounts of *CDKN1A* transcript showed an eightfold increase at 24 hours after MDMX depletion and remained increased (more than fivefold) at 48 hours and 72 hours after depletion of MDMX (Fig. 3A, bottom right panel). Amounts of p21 protein showed a continuous increase during the entire 72-hour period after MDMX depletion, which was p53-dependent (fig. S5). MDMX depletion also led to cell cycle arrest, as indicated by the increase in the percentage of cells in the $G_1$ phase of the cell cycle and a decrease in the percentage of cells in S phase (Fig. 3E, left panel). Suppression of p53 low-amplitude oscillations by a delayed expression of mKate2-*MDMX* (Figs. 2E and 3B) lowered amounts of p21 mRNA and protein (Fig. 3, C and D) and rescued cells from arrest (Fig. 3E, right panel). This indicates that the p53 oscillations after MDMX knockdown are responsible for maintaining p21 and cell cycle arrest.

The complexity of the p53 response to MDMX depletion prompted us to investigate how cells respond to DNA damage at different times after depletion of MDMX. We applied DNA damage either during the first phase (postmitotic pulse) or second phase (oscillations) of the p53 response and measured p53 dynamics and cell fate (Fig. 4A). When DNA damage was applied during the first phase (12 hours after transfection with MDMX siRNA), MDMX depletion sensitized cells to death, leading to 95% cell death as compared with 66% resulting from DNA damage alone (Fig. 4B). This increase in cell death may result from increased accumulation of p53 (Fig. 4, D, F and G, and fig. S6A) and increased transcription of apoptotic genes (Fig. 3A) during this phase. In sharp contrast, when DNA damage was applied during the second, oscillatory, phase of p53 dynamics (48 hours after MDMX

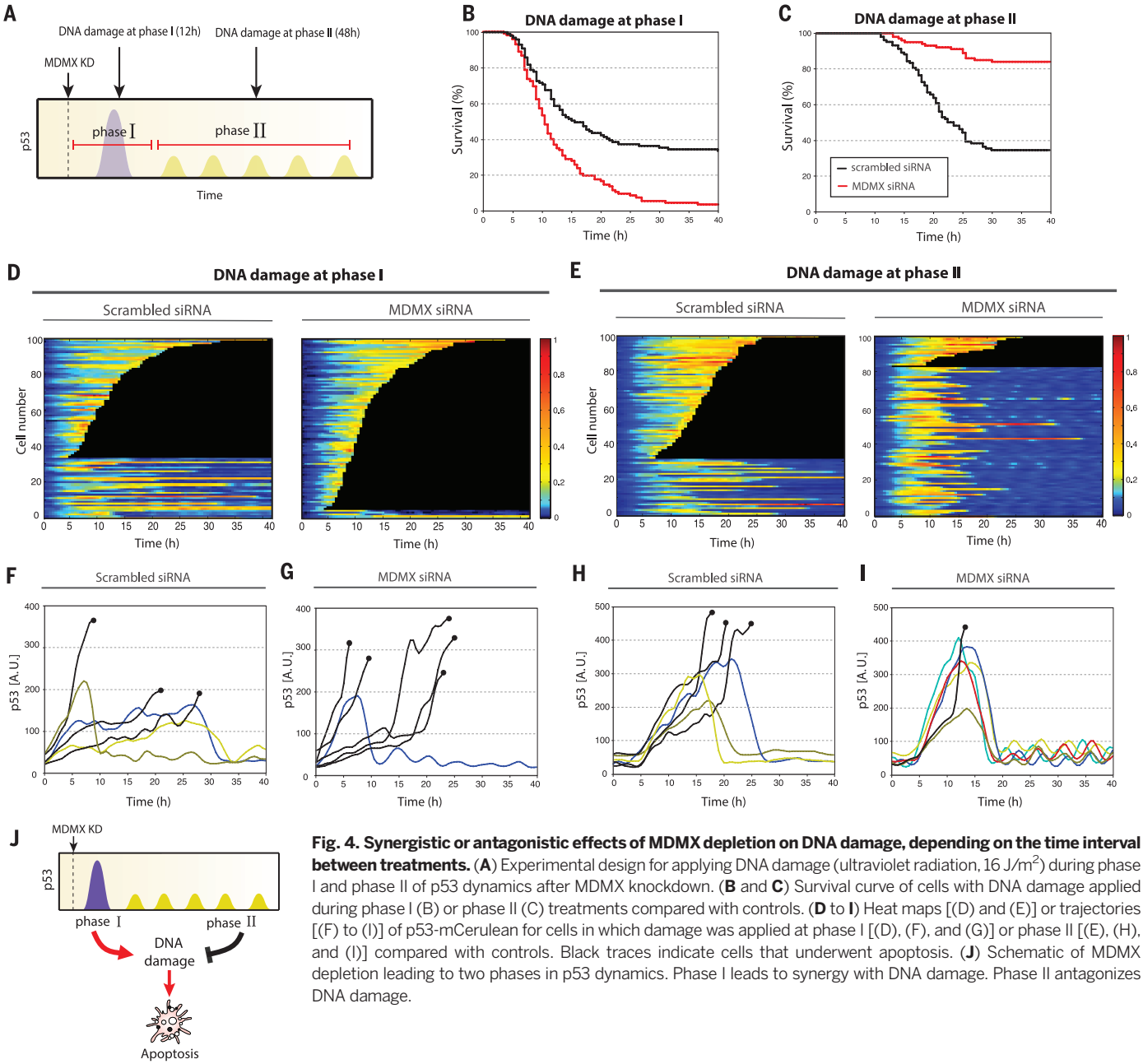


**Fig. 4. Synergistic or antagonistic effects of MDMX depletion on DNA damage, depending on the time interval between treatments.** (**A**) Experimental design for applying DNA damage (ultraviolet radiation, 16 J/m$^2$) during phase I and phase II of p53 dynamics after MDMX knockdown. (**B** and **C**) Survival curve of cells with DNA damage applied during phase I (B) or phase II (C) treatments compared with controls. (**D** to **I**) Heat maps [(D) and (E)] or trajectories [(F) to (I)] of p53-mCerulean for cells in which damage was applied at phase I [(D), (F), and (G)] or phase II [(E), (H), and (I)] compared with controls. Black traces indicate cells that underwent apoptosis. (**J**) Schematic of MDMX depletion leading to two phases in p53 dynamics. Phase I leads to synergy with DNA damage. Phase II antagonizes DNA damage.

was depleted) cell death was reduced (67 to 16%) (Fig. 4C). Similar schedule-dependent interactions were observed between MDMX suppression and four different chemotherapy agents (4NQO, doxorubicin, camptothecin, and actinomycin D) in MCF7 and the primary line RPE1 (fig. S7).

MDMX-depleted cells showed a similar amplitude of p53 accumulation to that in mock-treated cells when DNA damage was applied during phase II (Fig. 4, E, H, and I, and fig. S6B), indicating that the reduction in cell death is not caused by lower amounts of p53. Instead, we suggest that transcriptional regulation of genes by MDMX-induced p53 oscillations could make cells less susceptible to DNA damage. Indeed, p53 oscillations during the second phase after MDMX depletion induced accumulation of p21 and cell cycle arrest (Fig. 3, D and E), which provides protection from cell death (*17*). In addition, MDMX suppression led to a stronger activation of the pro-survival signal phospho-Akt after DNA damage and to a weaker accumulation of the pro-apoptotic protein PUMA as compared with those in MDMX-expressing cells (fig. S8). This suggests that, in addition to induction of p21 and cell cycle arrest by p53 oscillations, MDMX suppression shifts cells toward a pro-survival cellular state (fig. S8), which may also contribute to its protection from DNA damage–induced cell death.

The complexity of cellular signaling pathways makes it challenging to predict the response to a single perturbation, and even more challenging to predict responses to combined perturbations. In the context of combined therapeutic treatments, the schedule of administration can be crucial [Fig. 4J and (*1*, *18*, *19*)]. The results presented here unexpectedly show that the combination of DNA damage with MDMX inhibitors for cancer therapy has the potential either to improve cancer therapy or to blunt its effects. Our results have implications for the design of MDMX-combination drug regimes and perhaps for the design of combination therapies in general. Further consideration of treatment schemes in the context of other physiological rhythms, such as the cell cycle and circadian clock (*20*–*22*), can be critical for more precise and effective therapies. Such a detailed quantitative description of system behavior at the single-cell level can reveal hidden regulatory principles and the nature of cellular state changes in response to perturbations.

## REFERENCES AND NOTES


1. M. J. Lee *et al.*, *Cell* **149**, 780–794 (2012).
2. S. W. Morton *et al.*, *Sci. Signal.* **7**, ra44 (2014).
3. M. Wade, Y.-C. Li, G. M. Wahl, *Nat. Rev. Cancer* **13**, 83–96 (2013).
4. A. Gembarska *et al.*, *Nat. Med.* **18**, 1239–1247 (2012).
5. C. J. Brown, S. Lain, C. S. Verma, A. R. Fersht, D. P. Lane, *Nat. Rev. Cancer* **9**, 862–873 (2009).
6. J. A. Barboza, T. Iwakuma, T. Terzian, A. K. El-Naggar, G. Lozano, *Mol. Cancer Res.* **6**, 947–954 (2008).
7. F. Mancini *et al.*, *Int. J. Biochem. Cell Biol.* **42**, 1080–1083 (2010).
8. X. Wang, J. Wang, X. Jiang, *J. Biol. Chem.* **286**, 23725–23734 (2011).
9. J. E. Purvis *et al.*, *Science* **336**, 1440–1444 (2012).
10. B. Graves *et al.*, *Proc. Natl. Acad. Sci. U.S.A.* **109**, 11788–11793 (2012).
11. D. Reed *et al.*, *J. Biol. Chem.* **285**, 10786–10796 (2010).
12. G. Lahav *et al.*, *Nat. Genet.* **36**, 147–150 (2004).
13. A. Loewer, E. Batchelor, G. Gaglia, G. Lahav, *Cell* **142**, 89–100 (2010).
14. E. Batchelor, C. S. Mock, I. Bhan, A. Loewer, G. Lahav, *Mol. Cell* **30**, 277–289 (2008).
15. H. Kawai *et al.*, *J. Biol. Chem.* **278**, 45946–45953 (2003).
16. G. Lahav, *Adv. Exp. Med. Biol.* **641**, 28–38 (2008).
17. O. D. K. Maddocks *et al.*, *Nature* **493**, 542–546 (2013).
18. M. Behar, D. Barken, S. L. Werner, A. Hoffmann, *Cell* **155**, 448–461 (2013).
19. P. Lito, N. Rosen, D. B. Solit, *Nat. Med.* **19**, 1401–1409 (2013).
20. J. Bieler *et al.*, *Mol. Syst. Biol.* **10**, 739 (2014).
21. C. Feillet *et al.*, *Proc. Natl. Acad. Sci. U.S.A.* **111**, 9828–9833 (2014).
22. A. Sancar *et al.*, *FEBS Lett.* **584**, 2618–2625 (2010).



## ACKNOWLEDGMENTS

We thank A. G. Jochemsen, J. C. Marine, X. Wang, and J. Chen for sharing their experience and thoughts on MDMX regulation; R. Ward, S. Gruver, G. Gaglia, J. Porter, L. Bruett, and members of the Lahav laboratory for comments, support, and discussion; and the Nikon Imaging Center at Harvard Medical School for support with live cell imaging. This research was supported by National Institutes of Health grant GM083303 to G.L., grant F32GM105205 to S.C., and funding from the Novartis Institutes for Biomedical Research.


## SUPPLEMENTARY MATERIALS

www.sciencemag.org/content/351/6278/1204/suppl/DC1
Materials and Methods
Figs. S1 to S8
References (*23*–*25*)

12 May 2015; accepted 28 January 2016
10.1126/science.aac5610

CANCER THERAPY

# Disordered methionine metabolism in MTAP/CDKN2A-deleted cancers leads to dependence on PRMT5

**Konstantinos J. Mavrakis,[1]* E. Robert McDonald III,[1]* Michael R. Schlabach,[1]* Eric Billy,[2]* Gregory R. Hoffman,[1]* Antoine deWeck,[2] David A. Ruddy,[1] Kavitha Venkatesan,[1] Jianjun Yu,[3] Gregg McAllister,[1] Mark Stump,[1] Rosalie deBeaumont,[1] Samuel Ho,[1] Yingzi Yue,[1] Yue Liu,[1] Yan Yan-Neale,[1] Guizhi Yang,[1] Fallon Lin,[1] Hong Yin,[1] Hui Gao,[1] D. Randal Kipp,[1] Songping Zhao,[1] Joshua T. McNamara,[1] Elizabeth R. Sprague,[1] Bing Zheng,[3] Ying Lin,[4] Young Shin Cho,[1] Justin Gu,[4] Kenneth Crawford,[3] David Ciccone,[1] Alberto C. Vitari,[3] Albert Lai,[3] Vladimir Capka,[1] Kristen Hurov,[1] Jeffery A. Porter,[1] John Tallarico,[1] Craig Mickanin,[1] Emma Lees,[1] Raymond Pagliarini,[1] Nicholas Keen,[1] Tobias Schmelzle,[2]* Francesco Hofmann,[2]* Frank Stegmeier,[1]*† William R. Sellers[1]*†**

**5-Methylthioadenosine phosphorylase (MTAP) is a key enzyme in the methionine salvage pathway. The *MTAP* gene is frequently deleted in human cancers because of its chromosomal proximity to the tumor suppressor gene *CDKN2A*. By interrogating data from a large-scale short hairpin RNA–mediated screen across 390 cancer cell line models, we found that the viability of MTAP-deficient cancer cells is impaired by depletion of the protein arginine methyltransferase PRMT5. MTAP-deleted cells accumulate the metabolite methylthioadenosine (MTA), which we found to inhibit PRMT5 methyltransferase activity. Deletion of MTAP in MTAP-proficient cells rendered them sensitive to PRMT5 depletion. Conversely, reconstitution of MTAP in an MTAP-deficient cell line rescued PRMT5 dependence. Thus, MTA accumulation in MTAP–deleted cancers creates a hypomorphic PRMT5 state that is selectively sensitized toward further PRMT5 inhibition. Inhibitors of PRMT5 that leverage this dysregulated metabolic state merit further investigation as a potential therapy for MTAP/CDKN2A-deleted tumors.**

5-Methylthioadenosine phosphorylase (MTAP) participates in the methionine salvage pathway that metabolizes methylthioadenosine (MTA) to adenine and methionine. Because of its proximity to the tumor suppressor gene *CDKN2A* on human chromosome 9p21, the *MTAP* gene is deleted at high frequency in many human tumors, including 53% of glioblastomas, 26% of pancreatic cancers, and other tumor types (Fig. 1A). Given the critical role of MTAP in methionine metabolism, we hypothesized that the metabolic rewiring in response to MTAP loss may create new vulnerabilities.

[1]Novartis Institutes for Biomedical Research, Cambridge, MA 02139, USA. [2]Novartis Institutes for Biomedical Research, Basel CH-4002, Switzerland. [3]Novartis Institutes for Biomedical Research, Emeryville, CA 94608, USA. [4]China Novartis Institutes for Biomedical Research, Shanghai 201203, China.
*These authors contributed equally to this work. **†Corresponding authors. E-mail: william.sellers@novartis.com (W.R.S.); fstegmeier@ksqtx.com (F.S.)**


# Schedule-dependent interaction between anticancer treatments

Sheng-hong Chen *et al.*

*Science* **351**, 1204 (2016);
DOI: 10.1126/science.aac5610